Understanding multiple timescales in quantum dissipative dynamics: Insights from quantum trajectories

Matthew Gerry [1], Michael J. Kewming,[2] and Dvira Segal [1,3,*]

[1]*Department of Physics, University of Toronto, 60 Saint George St., Toronto, Ontario M5S 1A7, Canada*
[2]*School of Physics, Trinity College Dublin, College Green, Dublin 2, Ireland*
[3]*Chemical Physics Theory Group, Department of Chemistry and Centre for Quantum Information and Quantum Control, University of Toronto, 80 Saint George St., Toronto, Ontario M5S 3H6, Canada*

Open quantum systems with nearly degenerate energy levels have been shown to exhibit long-lived metastable states in the approach to equilibrium, even when modelled with certain Lindblad-form quantum master equations. This is a result of dramatic separation of timescales due to differences between Liouvillian eigenvalues. These metastable states often have nonzero coherences that die off only in the long-time limit once the system reaches thermal equilibrium. We examine two distinct situations that give rise to this effect: one in which dissipative dynamics couple together states only within a nearly degenerate subspace, and one in which they give rise to jumps over finite-energy splittings, between *separate* nearly degenerate subspaces. We find, in each case, that a change of basis can often lead to a representation that more naturally captures the impact of the system-bath interaction than does the energy eigenbasis, revealing that separate timescales are associated with separate processes (e.g., decoherence into a nonenergy eigenbasis, decay of population correlations to the initial state). This approach is paired with the inspection of quantum trajectories, which further provide intuition as to how open system evolution is characterized when coherent oscillations, thermal relaxation, and decoherence all occur simultaneously.

I. INTRODUCTION

Open quantum systems have been observed to exhibit, in some cases, a dramatic separation of timescales while relaxing towards equilibrium. Formally, this is attributed to significant differences in the magnitudes of different Liouvillian eigenvalues [1,2]. The phenomenon has received much attention in the context of anomalous relaxation, or the "quantum Mpemba effect", which aims to speed up the approach to equilibrium by reducing or eliminating the slowest timescales from the evolution [3–6]. In other studies, it has been considered whether intermediate metastable states that arise due to this timescale separation can offer advantages in applications such as quantum thermometry [7]. Generically, the long-lived metastable state that is reached in the relaxation towards equilibrium exhibits coherences between energy eigenstates, which die off only over the longest timescale of the dynamics as the system reaches its thermal state [8–10].

The question of how coherence may be maintained over long time periods in open quantum systems has garnered much interest in recent years, particularly as many hope for advances in the field of quantum information processing, where it will be crucial to be able to do so [11]. The significance of coherences has also been investigated in the context of quantum transport and quantum thermodynamics, where it has been questioned whether they can lead to improved performance of thermal machines [12–15], or play a role in the violation of cost-precision tradeoff relations [16–18]. Other studies have considered the role of coherence in biological processes, including photosynthesis [19,20] and vision [21,22].

Quantum master equations (QMEs) may be used to describe the behavior of open quantum systems in an attempt to capture the effects of coherence. Such equations, when derived from microscopic principles (e.g., the Redfield equation), do not, in general, preserve positivity of the reduced density operator [23,24] or satisfy fluctuation symmetry [25,26]. The remedy for this is to obtain equations of Gorini-Kossakowski-Lindblad-Sudarshan form [27–30]. This is often achieved by making the secular approximation and eliminating oscillating terms in the Redfield equation. However, this approach neglects any complicated interdependence between eigenstate populations and coherences that may arise for systems with eigenstates close in energy [31].

GKLS-form master equations that are obtained without making the full secular approximation have been derived to describe dynamics more accurately in the presence of nearly degenerate levels [31–35]. The so-called "unified" quantum master equation (UQME), which shall be our focus, is obtained from the Redfield equation by removing rapidly

*Contact author: dvira.segal@utoronto.ca

oscillating terms but keeping slowly oscillating terms—that is, those terms oscillating at frequencies set by the energy differences between pairs of nearly degenerate states. GKLS form is achieved by neglecting these small energy splittings in the calculation of bath-induced transition rates [31], resulting in a positivity-preserving, thermodynamically consistent [26,36] description that approximates the Redfield equation well in the presence of near degeneracies.

For open quantum systems with sets of nearly degenerate levels—those for which long-lived coherences tend to arise during the relaxation to equilibrium—there are, broadly, two situations of interest. Each can arise in isolation or both simultaneously, as determined by the form of the system-bath interaction. In the first, the dissipative dynamics couple together states within a nearly degenerate subspace. Such dynamics cause no change to the expectation value of the system Hamiltonian larger than the order of the small energy splitting. A simple example of such a situation would be a nearly degenerate two-level system coupled to a thermal bath in a manner that leads to transitions that build coherence between the levels.

In the second situation, dissipative dynamics lead the system to jump *between* distinct nearly degenerate subspaces, such that the jumps themselves are associated with a finite-energy splitting and the timescales for relaxation generally have explicit temperature dependence. This latter case is exemplified by the "V" model, which has a pair of nearly degenerate excited states separated by a finite-energy gap to a ground state. This model has been used as a paradigm for certain atomic systems in quantum optical studies [37,38], as well as nitrogen vacancy centres [39]. When studied using the Redfield equation, it has been found to exhibit dramatically distinct timescales during relaxation towards equilibrium, including long-lived coherences in the metastable state [8,10,40]. It has also shown coherences at steady state in nonequilibrium situations [41,42].

The dramatic separation of timescales, and associated long-lived coherences, in this model's relaxation to equilibrium is captured by the UQME, both in numerical simulations and approximate methods for obtaining analytic solutions to the master equation [2,26,42]. Mathematically, this effect may be attributed to the fact that the eigenvalues of the Liouvillian describing the system's time evolution span multiple orders of magnitude [2]; however, this explanation falls short in delivering intuition for the physical processes underlying the phenomenon at hand. Past studies have similarly understood interesting features of dynamics by means of the spectrum of the Liouvillian, for instance, in investigating the phenomenon of Liouvillian exceptional points [43,44]. Long-lived coherences like those that we focus on here have also been understood in the context of Fano coherences, which arise due to interference associated with distinct transitions from a single initial state [40,45], and for which intuition has been found through an effective decoherence rate model [46,47].

We will work to gain intuition in this context by studying systems with nearly degenerate states through quantum trajectories. Quantum trajectories, a concept with a longstanding history in quantum optics, were formally developed to depict quantum systems undergoing continuous measurements

[48–51]. In this scenario, the measurement process results in the stochastic evolution of a given trajectory. Averaging over many such trajectories recovers the ensemble average, described by a GKLS-form master equation.

To be more precise, a quantum trajectory is obtained by "unraveling" the master equation: examining a specific exemplary sequence of "jumps" and describing the evolution of the reduced density operator conditioned on the sequence ρ_c. This evolution occurs discontinuously at random instants when jumps happen. If the interaction with the environment involves continuous measurement (e.g., a detector in the environment clicks each time a jump occurs), ρ_c can be understood as the system's state conditioned upon a particular sequence of clicks. Taking the ensemble average of conditional density operators over the possible sequences then recovers the system's reduced density operator ρ. Unraveling frameworks of the quantum master equations that behave as expected under ensemble averaging are nonunique; different approaches have been applied, e.g., in Refs. [52,53]. The methodology we employ here offers physical insight into the dramatic separation of timescales seen in the relaxation towards equilibrium.

In this study, we consider minimal models that exhibit dramatically different timescales and long-lived coherences during their relaxation towards equilibrium. Our objective is to root these phenomena in underlying physical processes. Using the UQME—a natural choice of GKLS master equation, which captures the timescale effects—we investigate the dynamics of these systems as they thermalize. We build insight by carrying out the analysis not only in the energy eigenbases of the systems considered, but also in alternate bases that more naturally reflect the way the system-bath interaction manifests in the evolution of the state. This approach also lends itself elegantly to the unraveling of the master equation to observe quantum trajectories, which, in turn, help to further paint the picture of why separate timescales emerge in the overall dynamics. We do note, however, that the measurement operators do not constitute a clearly defined measurement process, but rather that the unravelled dynamics can shed light onto the separation of timescales. Similar strategies linking quantum trajectories with master equations have been applied in characterizing metastability in quantum systems [54–57], and studying open quantum systems subject to reset processes [58].

In Sec. II, we consider the case where dissipative dynamics act within a nearly degenerate subspace and work to build intuition for the physical processes underlying dramatic timescale separation during the relaxation to equilibrium. In Sec. III we turn our attention to the case in which dissipative dynamics act between distinct nearly degenerate subspaces, and identify and explain analogous timescale separation. In Sec. IV we summarize our findings and discuss how they are situated amongst a broader set of questions.

II. DISSIPATIVE DYNAMICS WITHIN A NEARLY DEGENERATE SUBSPACE

A. Setup

In order to probe the case in which dramatically different relaxation timescales occur as a result of dissipative dynamics
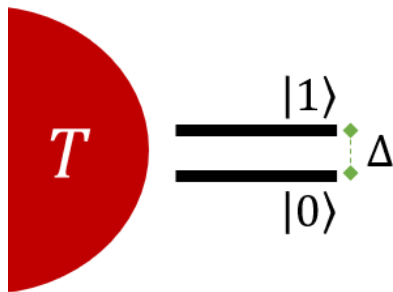
FIG. 1. Level diagram for the two-level system with splitting Δ, coupled to a bosonic bath at temperature T via the system-bath part H_{SB} of the Hamiltonian.

acting within a nearly degenerate subspace, we consider a basic model consisting of a spin (two-level system) coupled weakly to a reservoir. The full system plus environment is described by the Hamiltonian,

$$H = H_S + H_B + H_{SB}. \tag{1}$$

The system Hamiltonian is

$$H_S = \frac{\Delta}{2}(|1\rangle\langle 1| - |0\rangle\langle 0|). \tag{2}$$

The level diagram for this model, along with the bath, is depicted in Fig. 1.

H_{SB} describes the coupling between the system and bath, and is of the simple form

$$H_{SB} = S \otimes B \tag{3}$$

where S is an operator acting solely on the system Hilbert space, and B, on the bath.

Crucially, the "system part" of the interaction Hamiltonian is given by

$$S = \frac{1}{\sqrt{2}}(|0\rangle\langle 0| - |1\rangle\langle 1| + |0\rangle\langle 1| + |1\rangle\langle 0|). \tag{4}$$

In the energy eigenbasis, this is represented by a matrix $\mathbf{S} = (\sigma_x + \sigma_z)/\sqrt{2}$. This model, with levels that are not nearly degenerate relative to temperature, was considered in several studies with a focus on the survival of coherences in the steady state [59]. In Ref. [60] the model captured the steady state of a double quantum dot charge qubit. In nonequilibrium setups, the model exemplified novel heat transport effects beyond weak coupling [61].

We wish to derive the UQME for this system, which consists of transition rates whose specific values depend on the properties of the bath. These are obtained by evaluating the rates of the Redfield equation, which are, in general, functions of two distinct frequencies, at only the average of the two arguments. This captures the assumption of near degeneracy by effectively neglecting the difference between the two energy splittings and reduces the rate to a function of a single frequency [31], i.e.,

$$\gamma(\omega_1, \omega_2) \to \gamma(\omega) \equiv \gamma(\omega, \omega), \tag{5}$$

where $\omega \equiv (\omega_1 + \omega_2)/2$. Such rates can be determined for bosonic or fermionic baths, and for any form of the spectral density. To probe the phenomenon of dramatic timescale

separation for this two-level system, we require only one additional assumption: that we work in the limit of $\Delta \ll T$. That is, the two levels are nearly degenerate relative to the energy scale associated with the temperature, justifying the approximation described by Eq. (5).

In this case, the only transition rate describing the dissipative dynamics under the UQME is the one where the argument goes to zero,

$$\gamma \equiv \lim_{\omega \to 0} \gamma(\omega). \tag{6}$$

The lack of any large energy splittings in the system means that no terms in the Redfield equation are discarded to obtain the unified QME. The UQME is obtained from Redfield simply by taking all transition rates to the approximate value γ. In the Schrödinger picture, the UQME is given by

$$\frac{d\rho}{dt} = \mathcal{L}\rho = -i[H_S, \rho] + \mathcal{D}[L]\rho, \tag{7}$$

where $\rho \equiv \mathrm{Tr}_B[\rho_{\mathrm{tot}}]$ is the system reduced density operator, and

$$\mathcal{D}[L]\rho = L\rho L^{\dagger} - \tfrac{1}{2}\{L^{\dagger}L, \rho\}. \tag{8}$$

There is only one dissipator corresponding to a single collapse, or "Lindblad", operator, which is directly proportional to the system part of the interaction Hamiltonian,

$$L = \sqrt{\gamma}S. \tag{9}$$

While it is clear that Eq. (7) is of Lindblad form, since the single positive value γ clearly amounts to a positive semidefinite "matrix", this is in contrast to typical uses of fully secular quantum master equations, where there are often many collapse operators, and they tend of be of the form of projectors onto, or jumps between, energy eigenstates. Nonetheless, Eq. (7) describes evolution of the density operator for an ensemble.

The evolution at the trajectory level, however, is described by a stochastic jump equation [49],

$$d\rho_c = -\mathcal{H}[iH_S + \tfrac{1}{2}L^{\dagger}L]\rho_c dt + dN(t)\mathcal{G}[L]\rho_c, \tag{10}$$

where $dN(t)$ is a stochastic Poisson increment satisfying $dN(t)^2 = dN(t)$ and ρ_c is the conditioned density matrix. The two superoperators are defined by

$$\mathcal{G}[X]\rho = \frac{X\rho X^{\dagger}}{\mathrm{Tr}[X\rho X^{\dagger}]} - \rho,$$

$$\mathcal{H}[X]\rho = X\rho + \rho X^{\dagger} - \mathrm{Tr}[X\rho + \rho X^{\dagger}]. \tag{11}$$

Each detection event corresponds to a quantum jump given by the superoperator $\mathcal{G}[L]$. The average jump rate is given by $\mathrm{E}[dN(t)] = \mathrm{Tr}[L\rho L^{\dagger}]dt$, where $\mathrm{E}[X]$ denotes a classical average over stochastic trajectories. Thus, when $dN(t) = 0$, the evolution of the system will be governed by the "null-measurement" term—corresponding to the first term in Eq. (10). However, when a jump occurs the state is instantly updated according to the projection onto L as determined by the second term. Given the form of the interaction, in contrast to the case of coupling described by σ_z or σ_x only, we note that the state immediately after a jump exhibits coherence in the energy eigenbasis. Furthermore, since for our choice of interaction $L^{\dagger}L = \gamma I$, we have that $\mathrm{Tr}[L\rho L^{\dagger}] = \gamma$, simplifying the

normalization that must be carried out following a quantum jump, as described by Eq. (10).

While this assumption is by no means necessary, we consider, for the purpose of calculations, a bosonic bath, with

$$H_B = \sum_k \omega_k b_k^\dagger b_k, \tag{12}$$

where b_k is the annihilation operator for a mode k with energy ω_k. The bath is taken to be at thermal equilibrium with temperature T, so the number operators satisfy $\langle b_k^\dagger b_k \rangle = n(\omega_k)$, with $n(\omega) = (e^{\beta\omega} - 1)^{-1}$, the Bose-Einstein distribution at inverse temperature $\beta \equiv 1/T$ (we take the Boltzmann constant, $k_B = 1$). The bath operator that couples to the system is chosen to represent displacements of the bath modes, $B = \sum_k g_k(b_k^\dagger + b_k)$ with g_k as the microscopic coupling energies. From that, the transition rate appearing in the UQME is given by

$$\gamma = \lim_{\omega \to 0} n(\omega)\mathcal{J}(\omega) \tag{13}$$

where $\mathcal{J}(\omega) = 2\pi \sum_k g_k^2 \delta(\omega - \omega_k)$ is the spectral density of the bath. One possible choice would be an Ohmic bath, for which $\mathcal{J}(\omega) = a\omega$, and we have $\gamma = aT$. However, any choice of spectral density for which γ takes on a finite value is sufficient to observe the phenomena we investigate here. We emphasize again that the bath may be made of other constituents, such as fermions, with the bath operator B representing electron-hole pair excitations. The resulting rate would be modified from Eq. (13) [62], but the dynamics (for the same value of the rate constant) would be the same. The only requirement from the bath here is that it can exchange energy with the system.

B. Energy eigenbasis

We can write the equations of motion for the distinct elements of ρ in the energy eigenbasis as given by the unified quantum master equation. It is convenient to define the "polarization", $P = (\rho_{11} - \rho_{00})/2$. We use the superscripts R and I to denote the real and imaginary parts of complex-valued matrix elements. Utilizing the condition of normalization to reduce the system down to three equations, we have

$$\dot{P} = -\gamma\left(P + \rho_{10}^R\right),$$
$$\dot{\rho}_{10}^R = -\gamma\left(P + \rho_{10}^R\right) + \Delta\rho_{10}^I,$$
$$\dot{\rho}_{10}^I = -\Delta\rho_{10}^R - 2\gamma\rho_{10}^I. \tag{14}$$

These are the equations of motion consistent with using the UQME, and give results that show good agreement with full Redfield in the case where nearly degenerate levels are present [26]. However, other choices of how to truncate the Redfield equation have been employed in studies of similar models that emphasize other phenomena, such as coherences that may arise at steady state [59,60]. Critically, any choice that eliminates the coupling of populations to coherences in the energy eigenbasis, as is seen here, will not give rise to sets of dramatically different timescales in the approach to equilibrium. Note that Eq. (14) does not include the effect of the Lamb shift Hamiltonian. Including the Lamb shift does not impact the phenomena of dramatic timescale separation,

though it does have some qualitative effects on the results, as we discuss in the Appendix.

Given a choice of initial state, we can obtain analytic expressions for elements of ρ as a function of time by solving for the eigenvalues of the Liouvillian up to leading order in Δ. Following the approach of Ref. [2], we treat the Δ-dependent part of $\mathcal{L}$ as a perturbation, first solving for the eigenvalues of the "unperturbed" Liouvillian and then obtaining the order-Δ correction only for the eigenvalue that vanishes in the $\Delta \to 0$ limit. Supposing the system is initially in its ground state, $\rho(0) = |0\rangle\langle 0|$, we obtain the following expressions for the population of the excited state, $\rho_{11} = P + 1/2$, and the real part of the coherence, ρ_{10}^R, as functions of time:

$$\rho_{11}(t) = \frac{1}{2} - \frac{1}{4}(e^{-\frac{\Delta^2}{4\gamma}t} + e^{-2\gamma t}),$$
$$\rho_{10}^R(t) = \frac{1}{4}(e^{-\frac{\Delta^2}{4\gamma}t} - e^{-2\gamma t}). \tag{15}$$

Note that our analytic approach is not sufficient to solve for $\rho_{10}^I(t)$ with this particular choice of initial state, since it is initially zero and thus, by Eq. (14), the leading order contribution to its evolution is of order Δ. It is not valid to treat contributions of this order as perturbations.

Present in both expressions of Eq. (15) are two distinct timescales, $\tau_1 = 4\gamma/\Delta^2$ and $\tau_2 = 1/(2\gamma)$, corresponding to the reciprocals of the nonzero eigenvalues of the Liouvillian for this system, up to leading order in Δ. This describes evolution in the relatively short term to a metastable state, which exhibits nonzero coherence, before evolving to the true steady state of the system, which is the maximally mixed state $\rho_\infty = I_2/2$, where I_2 is the identity operator on a two-dimensional space. This is also the expected thermal state for this system, once again neglecting order-Δ contributions. This behavior is demonstrated in Fig. 2. Furthermore, while different choices of the initial state lead to different functional forms for the elements of ρ, the same timescales τ_1 and τ_2 arise independently of this choice, with the exception of trivial cases such as evolution beginning in the steady state.

C. Alternate basis

We take the fact that both timescales, τ_1 and τ_2, show up in the expressions for both the populations and coherence in the energy eigenbasis as motivation to transform to a new basis in hopes of gaining some insight into the physical origin of separate timescales. Namely, we identify the unitary matrix $\mathbf{V}$, which diagonalizes the Lindblad operator, i.e.,

$$\mathbf{L} = \mathbf{V}\tilde{\mathbf{L}}\mathbf{V}^{-1}, \tag{16}$$

where bold-faced, sans-serif symbols denote basis-dependent matrix representations of their associated operators. As such, $\mathbf{L}$ and $\tilde{\mathbf{L}}$ are the matrices representing L in the energy eigenbasis and new basis, respectively, with the latter diagonal. We find $\mathbf{V}$ to be given by

$$\mathbf{V} = \frac{i}{\sqrt{2}}\begin{pmatrix} -(1 - 1/\sqrt{2})^{1/2} & (1 + 1/\sqrt{2})^{1/2} \\ [2(1 - 1/\sqrt{2})]^{-1/2} & [2(1 + 1/\sqrt{2})]^{-1/2} \end{pmatrix}, \tag{17}$$

and the collapse operator is simply represented as $\tilde{\mathbf{L}} = -\sqrt{\gamma}\sigma_z$. We denote the new basis states $\{|\psi_+\rangle, |\psi_-\rangle\}$; they
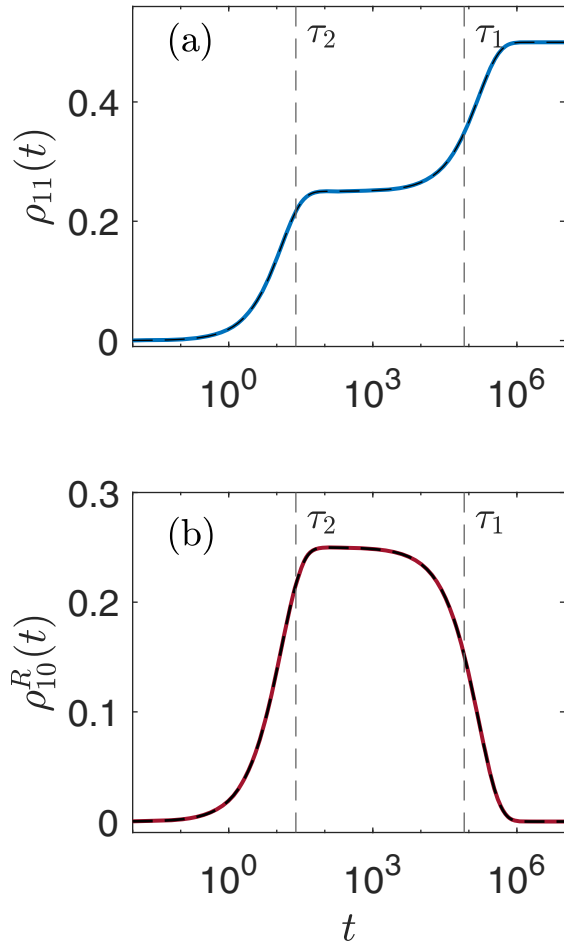
FIG. 2. (a) The excited state population and (b) the real part of the eigenstate coherence as a function of time, for a two-level system initially in the ground state, Eqs. (14) and (15). Analytical results from the perturbative method (dashed) are plotted along with numerical values obtained using the full unified QME (solid), showing good agreement. The two characteristic timescales, τ_1 and τ_2, describing the stages of relaxation towards equilibrium are shown as vertical-dashed lines. Calculations are carried out with $\Delta = 0.001$, $T = 1$, and $a = 0.02$, with a the dimensionless coupling coefficient as defined below Eq. (13).

are related to the energy eigenstates via

$$|\psi_\pm\rangle = \frac{i}{\sqrt{2}}\left(\pm\sqrt{1 \pm \frac{1}{\sqrt{2}}}|0\rangle + \frac{1}{\sqrt{2}}\frac{1}{\sqrt{1 \pm \frac{1}{\sqrt{2}}}}|1\rangle\right). \quad (18)$$

The system Hamiltonian is clearly not diagonal in this basis. It is expressed in terms of the new basis states as

$$H_S = \frac{1}{\sqrt{2}}\frac{\Delta}{2}(|\psi_-\rangle\langle\psi_-| - |\psi_+\rangle\langle\psi_+|$$
$$+ |\psi_+\rangle\langle\psi_-| + |\psi_-\rangle\langle\psi_+|). \quad (19)$$

The benefit of working in this new basis is that it offers a straightforward physical interpretation of the effect of the dissipative part of the dynamics at the trajectory level. At random instances in time, characterized by the rate γ, a "jump" occurs, taking the system to a new state. This transition amounts to

flipping the signs of the off-diagonal elements of ρ_c in the new basis, with no change to the diagonal elements. That is, the system-bath interaction can be understood as giving rise to pure decoherence. However, this decoherence is into a basis other than the energy eigenbasis, and is therefore paired with Rabi oscillations between basis states.

The fact that the system-bath Hamiltonian couples together states only within a nearly degenerate subspace is a requirement for the interaction to be interpreted in this way. A finite-energy splitting would require distinct upward and downward transition rates, leading to different Lindblad operators, which would not be simultaneously diagonalizable. In other words, there would be finite-energy changes associated with the dissipative dynamics, amounting to a relaxation process, rather than the pure dephasing we encounter here, which conserves the energy of the system up to leading order in Δ. The presence of just a single Lindblad operator proportional to the interaction Hamiltonian guarantees its diagonalizability, i.e., the existence of a basis in which it can be interpreted as describing pure decoherence [29]. This implies that, while we have focused for our examples on a specific form for the system part S of H_{SB}, the relevant basis could be identified given any choice of Hermitian operator S, provided all else is held equal.

To determine how the state of our exemplary system evolves as a function of time under the same conditions as in Sec. II B, we obtain the initial state (ground state of H_S) in this new basis. As a matrix,

$$\tilde{\boldsymbol{\rho}}(0) = \mathbf{V}^{-1}\boldsymbol{\rho}(0)\mathbf{V} = \frac{1}{2}\left(I - \frac{1}{\sqrt{2}}(\sigma_x + \sigma_z)\right). \quad (20)$$

We obtain an expression for the top-left matrix element of $\tilde{\boldsymbol{\rho}}$, which, due to the change of basis, represents the population not of the *ground* state, but rather, of the state $|\psi_-\rangle$. We denote this ρ_{--} and the population of state $|\psi_+\rangle$, ρ_{++}. We also solve for the real and imaginary parts of the coherence between the new basis states, $\rho_{+-} \equiv \langle\psi_+|\rho|\psi_-\rangle$. This amounts to solving the UQME, which takes the form of the following set of equations, where we define the variable $\tilde{P} \equiv (\rho_{--} - \rho_{++})/2$,

$$\dot{\tilde{P}} = \frac{\Delta}{\sqrt{2}}\rho_{+-}^I,$$

$$\dot{\rho}_{+-}^R = -2\gamma\rho_{+-}^R - \frac{\Delta}{\sqrt{2}}\rho_{+-}^I,$$

$$\dot{\rho}_{+-}^I = -\frac{\Delta}{\sqrt{2}}(\tilde{P} - \rho_{+-}^R) - 2\gamma\rho_{+-}^I. \quad (21)$$

Again, the effect of the Lamb shift is not captured in these equations, but discussed in the Appendix.

Using the same perturbative method with which we solved for the matrix elements in the eigenbasis, we obtain expressions for ρ_{--} and ρ_{+-}^R as functions of time, transforming back to the density matrix elements from the solution for $\tilde{P}$,

$$\rho_{--}(t) = \frac{1}{2} - \frac{1}{2\sqrt{2}}e^{-\frac{\Delta^2}{4\gamma}t},$$

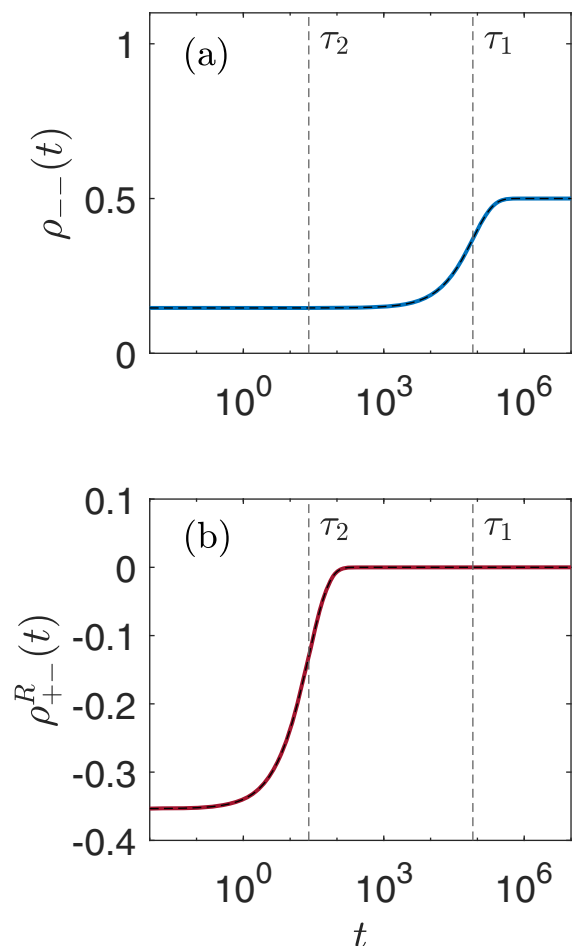$$\rho_{+-}^R(t) = -\frac{1}{2\sqrt{2}}e^{-2\gamma t}. \quad (22)$$

FIG. 3. (a) The level population and (b) real part of the coherence in the alternate basis [Eqs. (21) and (22)] as a function of time, starting from the ground state of the system Hamiltonian. The solid curves represent the results of solving the master equation numerically, while the dashed-black curves are the approximate analytic expressions. The two timescales are shown as vertical-dashed lines. Parameter values are the same as in Fig. 2.

Once again, variations in ρ^I_{+-} are of order Δ and smaller and thus are not captured by the analytic methods, so we focus on ρ_{--} and ρ^R_{+-} for the timescale analysis. In addition, as before, the maximally mixed state is approached in the long-time limit, as expected due to its basis independence.

As in Eq. (15), we note the two distinct timescales, τ_1 and τ_2. However, rather than both appearing in both expressions, τ_1 can be interpreted strictly as a timescale for the decay of populations in this basis towards their steady state values, while τ_2 is strictly a timescale for the decay of coherences to zero. This is demonstrated in Fig. 3, wherein the evolution of each element of ρ appears as simple exponential decay. It is still the case that the system first evolves to a quasi-steady state, where it remains while $\tau_2 < t < \tau_1$. In this basis, this state is characterized simply by the coherence having decayed but the populations remaining close to their initial values. The values plotted in Fig. 3 may be transformed back to the energy eigenbasis via the matrix **V**, to give results very similar to those obtained when solving the UQME directly in the energy eigenbasis.

D. Trajectory analysis

To gain some insight as to why the unified QME in this alternate basis gives rise to the behavior expressed by Eq. (22) and shown in Fig. 3, we can look at an example trajectory in this basis for the system under the evolution described. This is generated using the QuTip python library [63,64], and shown in Fig. 4. Averaging over such trajectories recovers the time evolution of the density operator plotted in Fig. 3 in the limit of an infinite sample size.

Since the system Hamiltonian is not diagonal in this basis, the unitary contribution to evolution under the UQME is characterized by Rabi oscillations with angular frequency Δ. In the absence of any interaction with the bath, this leads to oscillations of the off-diagonal elements along the *envelope* in Fig. 4(b), exactly out of phase with corresponding population oscillations. The interaction with the bath, however, causes the sign of the off-diagonal elements to flip at randomly timed jumps with rate γ. At the level of an ensemble, these sign-flipping events lead coherences to die off on the timescale τ_2, as while the initial state dictates that all trajectories begin with $\rho^R_{c,+-}(0) = -1/(2\sqrt{2})$, positive and negative values that arise after varying sequences of jumps lead to a result of zero when averaging over many trajectories. Conversely, these jumps help the populations remain closer to their initial values for longer than they would under isolated Rabi oscillations.

To understand this, we consider the evolution of ρ_c on the Bloch sphere, where the state is represented by a vector $\vec{s}$ with components $s_x = 2\rho^R_{c,+-}$, $s_y = 2\rho^I_{c,+-}$, and $s_z = \rho_{c,--} - \rho_{c,++}$. The coherent part of its time evolution, amounting to Rabi oscillations, is given by

$$\dot{\vec{s}} = \vec{\Omega} \times \vec{s}, \tag{23}$$

where $\times$ represents the cross product in three dimensions and $\vec{\Omega} = (\Delta/\sqrt{2}, 0, \Delta/\sqrt{2})^T$ is the so-called "drive vector". This is equivalent to the equations of motion, Eq. (21), but without the effects of dissipation. At the trajectory level, these effects are instead reflected in the random jumps that occur, over and above the evolution described by Eq. (23).

Our initial state corresponds to a vector in the lower-right quadrant of the xz plane, strictly antiparallel to $\vec{\Omega}$, as shown in Fig. 5(a). The state is stationary; it is, after all, the ground state of the system Hamiltonian. However, before long, a jump occurs, reflecting $\vec{s}$ across the z axis [Fig. 5(b)]. $\vec{s}$ is suddenly perpendicular to $\vec{\Omega}$, around which it begins to precess with angular frequency Δ, bringing it out of the xz plane into the $-y$ region. $\dot{s}_z \propto s_y$, so s_z begins to decrease, but only until the next jump takes the state into the $+y$ region. After this point, s_z begins to increase again, reversing the previous decrease [Fig. 5(c)]. Since $\gamma \gg \Delta$, changes to s_z (i.e., changes to the state *populations*) rarely have the opportunity to accumulate much before a jump occurs and they are undone. This is why, at short times, $\rho_{c,--}$ undergoes the jagged evolution around its initial value demonstrated in Fig. 4. Only on much longer timescales, on the order of τ_1, does the Bloch vector reach the vicinity of the equator, as in Fig. 5(d). This signifies that the correlations to the initial value of the populations have died off and the system is truly in a thermal state.

One may expect the coherences to exhibit similar behavior, since it is also the case that $\dot{s}_x \propto s_y$. The key difference is
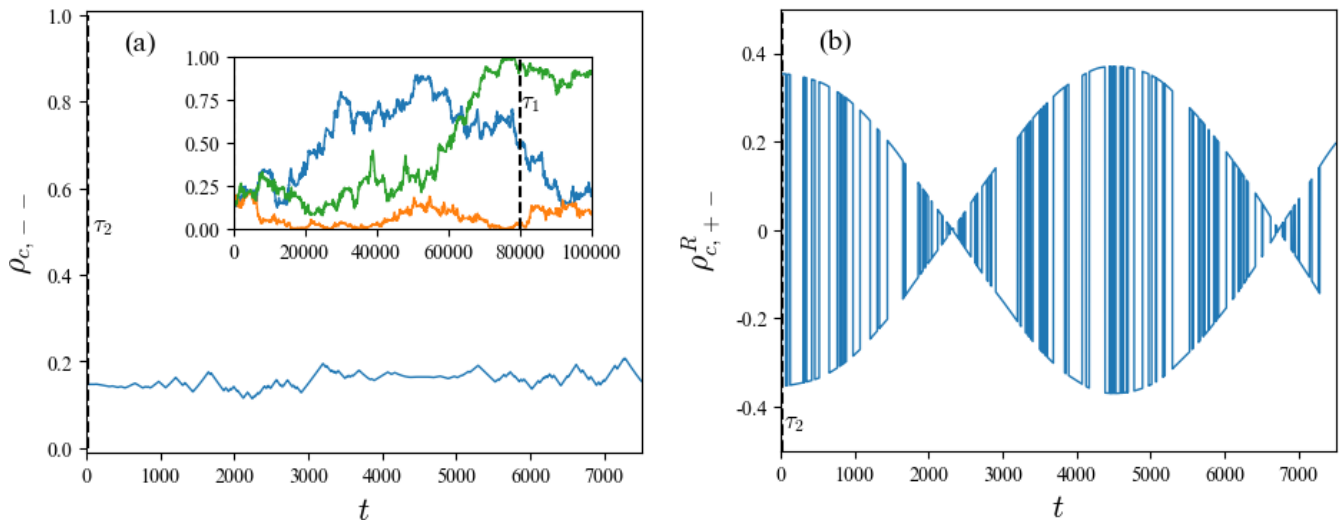
FIG. 4. A sample individual trajectory for (a) the population of $|-\rangle$ and (b) the real part of the coherence under the evolution described in Sec. II in the alternate basis [Eqs. (16)–(22)]. τ_2 is displayed in each panel as a vertical-dashed line, very close to the origin. Initial state and parameter values are the same as in Fig. 2. [Inset in (a)] The population evolution is shown over a longer time interval for three sample trajectories, demonstrating that all maintain similar values at short times. τ_1 is shown as a vertical-dashed line in the inset, by which time, correlations between the current and initial values are lost.

that while a jump does, therefore, lead $\dot{s}_x$ to change sign, so simultaneously does s_x *itself*. This allows changes to $|s_x|$ to accumulate seamlessly rather than being constantly undone, in a manner that effectively characterizes uninterrupted Rabi oscillations up to a frequently flipping sign (as in Fig. 4). It should be noted that the amplitude of these oscillations does change with the gradual changes to the populations.

Lasting changes to the populations do occur, however, as a result of fluctuations in the wait times between jumps. The population evolution is equivalent to simple harmonic motion with angular frequency Δ, but with the additional feature that the direction changes at random, as in a telegraph process. In the regime where $\gamma \gg \Delta$, this means the populations are

pinned close to their initial values for timescales much longer than $\sim 1/\Delta$. However, since the wait times between jumps can vary, correlations between the populations and their initial values do eventually die off. It can be shown that this decay of correlations occurs on a timescale proportional to $\gamma/\Delta^2 \propto \tau_1$ [65], in agreement with the expression for $\rho_{--}(t)$ given in Eq. (22). For times $t \gg \tau_1$, the populations are equally likely to take on any value, as suggested by the inset of Fig. 4. This effect can also be seen if the two-time correlation function of the Pauli-Z operator is derived directly in this basis for the two-level quantum system under consideration. This correlation function can be calculated using the quantum regression theorem [66], and it takes on the very
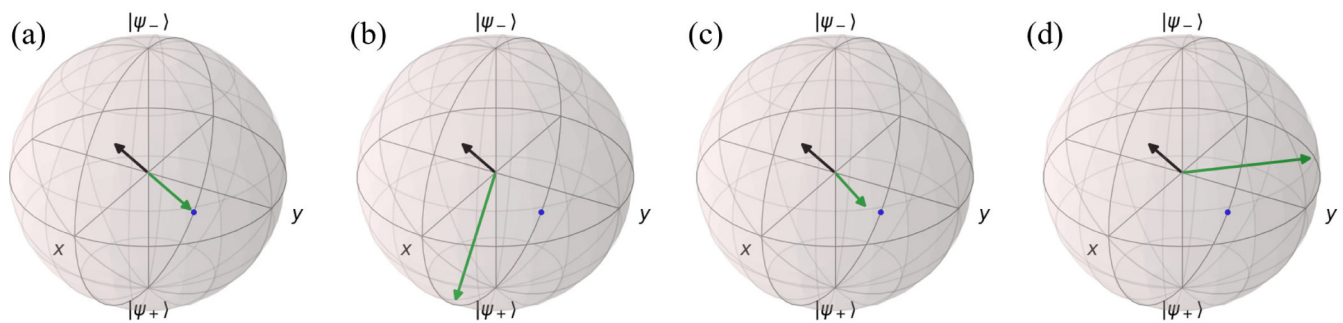

FIG. 5. Various snapshots of the evolution of one sample trajectory, depicted as a vector on the Bloch sphere (green), where the x, y, and z axes represent the real and imaginary parts of the coherence in the alternate basis, and the population polarization between states $|-\rangle$ and $|+\rangle$, respectively. The initial state is shown throughout as a blue dot. The "drive" vector $\vec{\Omega}$ about which the Bloch vector precesses in Rabi oscillations, is also shown (black). Note that this quantity has units of frequency, thus only its direction is meaningful as shown in these diagrams. (a) The initial state is the ground state, and is therefore stationary. (b) An instantaneous jump occurs after a time period of order τ_2, represented by a reflection of the Bloch vector across the z axis. There is now a finite angle between the Bloch vector and the drive vector, so Rabi oscillations proceed. (c) After another jump, the Bloch vector is slightly offset from its initial position, so the precession continues, albeit at a much slower rate. Jumps continue to occur at a rate set by the timescale τ_2. (d) After a time period on the order of τ_1, the Bloch vector is in the vicinity of the equator, indicating that, at the ensemble level, the system has reached the maximally mixed state, which corresponds to the true steady state for this system. Parameter values are the same as in Fig. 2.
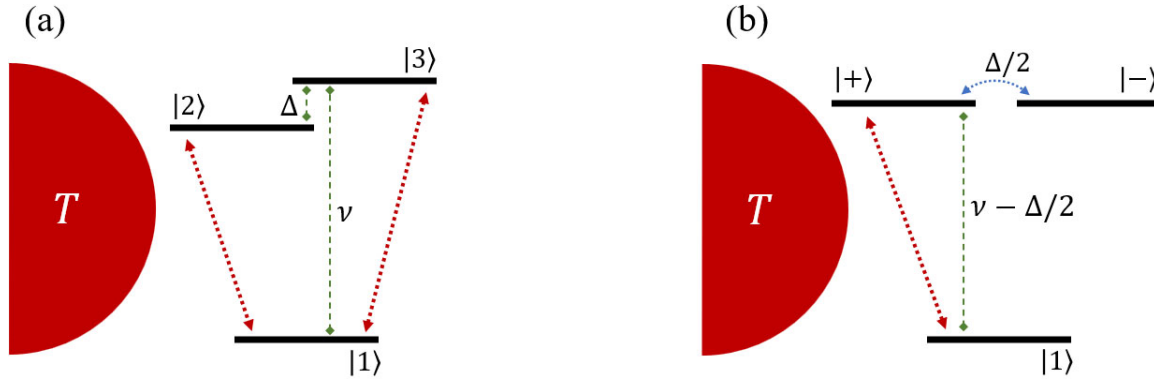
FIG. 6. (a) The V model represented in the energy eigenbasis, with states and energy splittings labeled. The bath excites transitions between the ground state and both excited states (red-dotted arrows). (b) The V model level diagram in the alternate basis. The bath only couples the ground state with $|+\rangle$ (red-dotted arrow), but $|+\rangle$ and $|-\rangle$ are coupled coherently with a tunneling amplitude $\Delta/2$ (blue-dotted arrow).

simple form,

$$\langle \sigma_z(t) \sigma_z(0) \rangle = e^{-\frac{\Delta^2}{4\gamma} t}. \tag{24}$$

Thus, the maximally mixed state is reached in the long-time limit, explaining the long-time behavior of the state regardless of the basis in which one chooses to study its evolution. The metastable state in the energy eigenbasis, characterized by intermediate values of both the populations and coherence, can now be understood as the basis-transformed version of the metastable state we have characterized here, where the coherences have died off quickly but the populations remain close to their initial values.

III. DISSIPATIVE DYNAMICS BETWEEN DISTINCT NEARLY DEGENERATE SUBSPACES

A. Setup and energy eigenbasis calculations

Another situation in which dramatic timescale separation and long-lived coherences arise is that in which dissipative dynamics lead a system to jump, over finite-energy splittings, into and out of distinct nearly degenerate subspaces. To investigate this situation, we consider a simple system fitting this description, the "V" model, which consists of one ground state and two nearly degenerate excited states. This system can exhibit long-lived transient coherences similar to those identified in the two-level model of Sec. II [8,22,40]. Unlike the previous model, however, these coherences arise not only in the high-temperature limit.

The system Hamiltonian for this model is

$$H_S = (\nu - \Delta)|2\rangle\langle 2| + \nu|3\rangle\langle 3|, \tag{25}$$

where $\Delta \ll \nu$. The ground state (zero energy) is labeled $|1\rangle$. The level diagram for this model is shown in Fig. 6(a). The structure of the Hamiltonian otherwise matches Eq. (3), but with the system part of the interaction Hamiltonian now given by

$$S = \frac{1}{\sqrt{2}}(|1\rangle\langle 2| + |1\rangle\langle 3| + \text{H.c.}) \tag{26}$$

where H.c. represents the Hermitian conjugate. The derivation of the unified QME for this model is analogous to that of

Sec. II; however, we identify two distinct collapse operators,

$$L_\downarrow = \sqrt{\frac{\gamma}{2}}|1\rangle(\langle 2| + \langle 3|),$$

$$L_\uparrow = \sqrt{\frac{e^{-\beta\nu}\gamma}{2}}(|2\rangle + |3\rangle)\langle 1|. \tag{27}$$

Note that these two operators represent jumps between levels separated by finite energy differences: namely, between the ground state and the coherent superposition of the two excited states given by $|+\rangle = (|2\rangle + |3\rangle)/\sqrt{2}$. This represents a major distinction from the situation considered in Sec. II, as transitions in this system are associated with finite energy changes in the bath, and therefore cannot be interpreted as pure decoherence into any basis. Indeed, the presence of a finite-energy splitting permits changes to the expectation value of the system Hamiltonian larger than order Δ as the system evolves. In general, the level populations of the initial state do not match those required for the Gibbs' state describing the system at equilibrium, and there *must* be some thermal relaxation that takes place in addition to any dephasing.

As for the two excited levels, we neglect energy differences of order Δ in defining the transition rates, allowing for the derivation of a Lindblad-form quantum master equation. We once again assume, merely for the purpose of calculations, that the bath is bosonic with Ohmic spectral density, giving the downward transition rate

$$\gamma(\nu - \Delta, \nu) \to \gamma \equiv \gamma(\nu, \nu) = \mathcal{J}(\nu)[n(\nu) + 1]$$
$$= a\nu[n(\nu) + 1]. \tag{28}$$

The associated rate for an upward transition is given by $\mathcal{J}(\nu)n(\nu) = e^{-\beta\nu}\gamma$, as reflected in the expression for $L_\uparrow$. The presence of the finite-energy splitting ν is further reflected by the distinction between the upward and downward transition rates, whose ratio exhibits temperature dependence satisfying detailed balance relations [29]. This temperature dependence will propagate through to temperature dependence of the relaxation timescales themselves.

Due to a symmetry of the system, the difference, $\rho_{22} - \rho_{33}$, between the populations of the two excited states decouples under the UQME from the rest of the dynamics and decays to zero with rate $\gamma/2$. We will consider
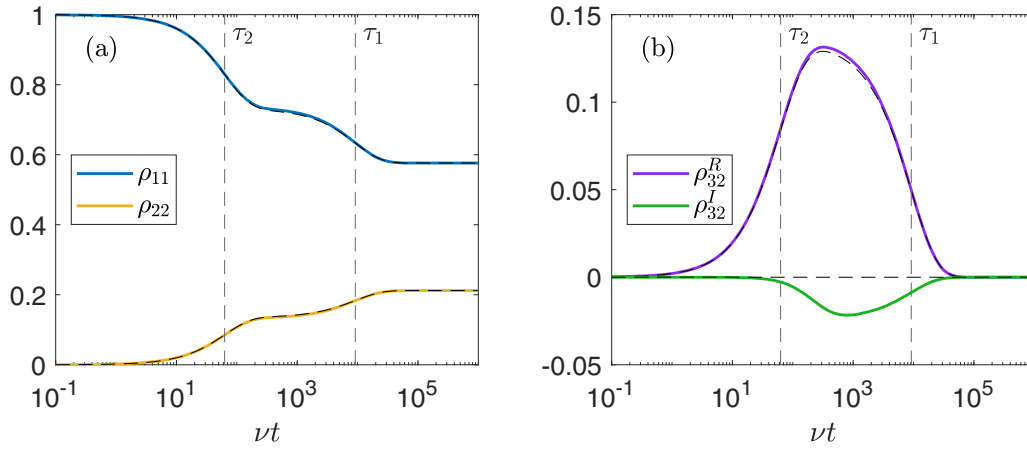
FIG. 7. (a) The populations of states $|1\rangle$ and $|2\rangle$ and (b) the real and imaginary part of the coherence ρ_{32} for the V model in the energy eigenbasis, initially in the ground state. Note that $\rho_{33}(t) = \rho_{22}(t)$ for all t, so only $\rho_{22}(t)$ is shown here. The dashed lines correspond to analytic perturbative calculations, showing close correspondence to the exact numerical values, with the exception of the imaginary part of the coherence, which the perturbative calculations do not capture. The two characteristic timescales are shown as vertical-dashed lines. $v = 1$, $\Delta = 0.001$, $a = 0.02$, and $T = 1$.

the case where the system begins in the ground state, $\rho(0) = |1\rangle\langle 1|$. Therefore, $\rho_{22}(0) = \rho_{33}(0) = 0$, and we have that $\rho_{33}(t) = \rho_{22}(t) = (1 - \rho_{11}(t))/2$ for all t. This allows the dynamics to reduce to a system of three homogeneous equations when we make a variable substitution, now defining $P \equiv (\rho_{33} + \rho_{22})/2 - e^{-\beta v}\rho_{11}$. We have

$$\dot{P} = -\gamma\left(\frac{1}{2} + e^{-\beta v}\right)(P + \rho_{32}^R),$$

$$\dot{\rho}_{32}^R = -\frac{\gamma}{2}(P + \rho_{32}^R) + \Delta\rho_{32}^I,$$

$$\dot{\rho}_{32}^I = -\Delta\rho_{32}^R - \frac{\gamma}{2}\rho_{32}^I. \tag{29}$$

Using the perturbative method outlined in Sec. II along with the assumption that the initial state is the ground state, we are able to obtain expressions for the ground-state population and the real part of the coherence,

$$\rho_{11}(t) = \frac{1}{\mathcal{Z}(\beta)} + \frac{e^{-\beta v}}{\mathcal{Z}_I(\beta)}\left(\frac{1}{\mathcal{Z}(\beta)}e^{-\frac{\mathcal{Z}(\beta)}{\mathcal{Z}_I(\beta)}\frac{\Delta^2}{\gamma}t} + e^{-\mathcal{Z}_I(\beta)\gamma t}\right),$$

$$\rho_{32}^R(t) = \frac{e^{-\beta v}}{2}\left(e^{-\frac{\mathcal{Z}(\beta)}{\mathcal{Z}_I(\beta)}\frac{\Delta^2}{\gamma}t} - e^{-\mathcal{Z}_I(\beta)\gamma t}\right), \tag{30}$$

where $\mathcal{Z}(\beta) = 1 + 2e^{-\beta v}$ is the partition function up to leading (zero) order in $\beta\Delta$. $\mathcal{Z}_I(\beta) = 1 + e^{-\beta v}$ is the analogous partition function for a two-level system with splitting v. As we will see, this quantity is relevant to describing the intermediate state of the system. In analogy to the two-level system, the perturbative method once again cannot capture the leading order of the evolution of the imaginary part of the coherence. We plot a selection of the matrix elements of $\rho(t)$ in Fig. 7 as determined by solving the unified QME numerically, alongside the predictions associated with these perturbative calculations. Here we can see a good level of accuracy for the elements that the analytic method is able to capture.

Similar to the two-level system discussed in Sec. II, we identify here two distinct timescales for the relaxation to

equilibrium, which scale in the same manner with the transition rate γ, and small splitting Δ. The V model, however, has a larger splitting v, which we do not assume is small relative to T. Therefore, the timescales depend additionally on temperature via the quantity βv, the magnitude of which we assume nothing about. They are given by

$$\tau_1 = \frac{\mathcal{Z}_I(\beta)}{\mathcal{Z}(\beta)}\frac{\gamma}{\Delta^2},$$

$$\tau_2 = \frac{1}{\mathcal{Z}_I(\beta)}\frac{1}{\gamma}. \tag{31}$$

Once again, this system exhibits long-lived coherences in the energy eigenbasis, which arise after the dynamics begin, and decay to zero only on the longer timescale τ_1. We note that these timescales are in agreement [42] with the results obtained using the Redfield equation in Refs. [8,40].

In an important contrast to the two-level system, the finite splitting v means that any bath-induced transition is necessarily accompanied by a non-negligible change in energy of the bath. Therefore, no change of basis can make the interaction with the bath "look like" pure decoherence—the Lindblad operators cannot be simultaneously diagonalized. Accordingly, there is no basis in which each element of the density matrix evolves with only a single timescale, as we have identified for the two-level system and show in Fig. 3.

B. Alternate basis and trajectory analysis

We can, however, make an argument that is similar in spirit, by transforming to the basis, $\{|1\rangle, |+\rangle, |-\rangle\}$, where $|\pm\rangle = (|2\rangle \pm |3\rangle)/\sqrt{2}$. The Lindblad operators then describe jumps between basis states,

$$L_{\downarrow} = \sqrt{\gamma}|1\rangle\langle +| \quad \text{and} \quad L_{\uparrow} = \sqrt{e^{-\beta v}\gamma}|+\rangle\langle 1|. \tag{32}$$

Furthermore, $|+\rangle$ and $|-\rangle$ are not energy eigenstates, and the Hamiltonian gives rise to Rabi oscillations between them. In

particular, the system Hamiltonian is

$$H_S = \left(\nu - \frac{\Delta}{2}\right)(|+\rangle\langle+| + |-\rangle\langle-|) + \frac{\Delta}{2}(|+\rangle\langle-| + |-\rangle\langle+|).$$

(33)

In this basis, the bath couples the ground state to the $|+\rangle$ level, which itself is coupled to the $|-\rangle$ site through a tunneling term $\Delta/2$. Furthermore, in this basis it is the real part of the coherence, $\rho_{+-}^R \equiv \mathrm{Re}[\langle+|\rho|-\rangle]$, that decouples from the rest of the dynamics. The UQME once again amounts to a system of three homogeneous equations. Making use of the variables $P_1 = (\rho_{++} - e^{-\beta\nu})/2$ and $P_2 = (\rho_{++} - \rho_{--})/2$, where $\rho_{\pm\pm} \equiv \langle\pm|\rho|\pm\rangle$, these are

$$\dot{P}_1 = -\gamma \mathcal{Z}_I(\beta) P_1 - \frac{\Delta}{2}\rho_{+-}^I,$$

$$\dot{P}_2 = -\gamma P_1 - \Delta\rho_{+-}^I,$$

$$\dot{\rho}_{+-}^I = \Delta P_2 - \frac{\gamma}{2}\rho_{+-}^I.$$

(34)

Using the same perturbative method of Ref. [2] to obtain expressions for the populations, ρ_{++} and ρ_{--}, of state $|+\rangle$ and $|-\rangle$, respectively, we find

$$\rho_{++}(t) = \frac{e^{-\beta\nu}}{\mathcal{Z}(\beta)} + \frac{e^{-\beta\nu}}{\mathcal{Z}_I(\beta)}\left(\frac{e^{-\beta\nu}}{\mathcal{Z}(\beta)}e^{-\frac{\mathcal{Z}(\beta)}{\mathcal{Z}_I(\beta)}\frac{\Delta^2}{\gamma}t} - e^{-\mathcal{Z}_I(\beta)\gamma t}\right),$$

$$\rho_{--}(t) = \frac{e^{-\beta\nu}}{\mathcal{Z}(\beta)}\left(1 - e^{-\frac{\mathcal{Z}(\beta)}{\mathcal{Z}_I(\beta)}\frac{\Delta^2}{\gamma}t}\right).$$

(35)

In analogy to the two-level system, the perturbative method does not capture the dynamics of ρ_{+-}^I since the leading order contribution to its evolution is of order Δ. Luckily, the populations in this basis are sufficient to draw the insights we want to discuss. We plot in Fig. 8 the populations obtained by solving the master equation numerically, alongside curves representing these expressions. Transforming the results plotted in Fig. 8 back into the energy eigenbasis yields behavior very close to the results of the direct eigenbasis calculations shown in Fig. 7.

Interestingly, only the longer timescale τ_1 appears in the expression for ρ_{--}. This can be understood as a result of the fact that $|-\rangle$ is isolated as the state that is not "included" in the dissipative dynamics, see Eq. (32). Bath-induced jumps from the ground state, which occur with a rate $e^{-\beta\nu}\gamma$, serve only to populate state $|+\rangle$ directly. Population can only arrive in $|-\rangle$ via the Rabi oscillations that take place after a jump up to $|+\rangle$. The period for these Rabi oscillations is proportional to $1/\Delta$, but the timescale for ρ_{--} to reach its steady-state population is increased to $\sim\gamma/\Delta^2$ by the fact that these Rabi oscillations are often quickly interrupted by a jump back down to the ground state, as shown in Fig. 9(a). Figure 9(b) displays an average of 50 distinct trajectories of the type depicted in Fig. 9(a), showing that averaging as such indeed recovers the nonconditional reduced density operator. Interestingly, the averaged trajectories for ρ_{11} and ρ_{++} exhibit far more noise than that for ρ_{--}, likely attributed to the special status of $|-\rangle$ as the state not directly involved in the dissipative dynamics, and thus not involved in the frequent jumps that occur as a consequence of the coupling to the bath.
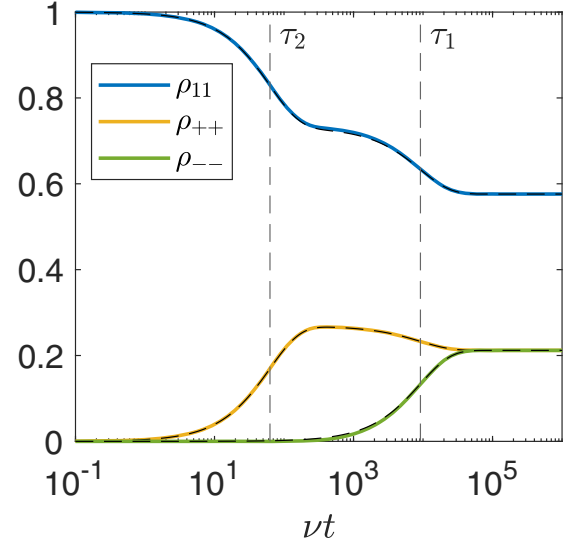

FIG. 8. Populations of the three levels of the V model in the $\{|1\rangle, |+\rangle, |-\rangle\}$ basis, starting from the ground state. The dashed curves represent the results of analytic perturbative calculations. As with the other setups considered, thermalization takes place over two distinct timescales. Here, only the slower timescale τ_1 shows up in the evolution of the population $\tilde{\rho}_{--}$, which is not directly involved in the dissipative dynamics. The two characteristic timescales are shown as vertical-dashed lines. Parameter values are the same as in Fig. 7.

The approach to equilibrium can be understood to happen in two distinct phases. The first is thermalization with respect to the larger energy gap ν, which occurs over a shorter timescale τ_2 set by the rate constant γ characterizing the dissipative dynamics. The second is the "mixing" of the two excited states $|+\rangle$ and $|-\rangle$, which happens over a slower timescale due to the constraints placed on the dynamics by the Hamiltonian. We can understand this by considering how we neglect the energy difference Δ between states $|2\rangle$ and $|3\rangle$ in describing the dissipative dynamics. Because of this, $\rho_{22} = \rho_{33}$ in the Gibbs state describing the system at equilibrium, i.e., the steady state is "maximally mixed" with respect to these two states. Thus, the 2×2 submatrix of ρ describing the excited states and their coherences is proportional to I_2 at equilibrium, and invariant under any change of basis that affects only these two states (like the one we have used).

The thermalization dynamics must therefore reflect both that (i) at steady state $\rho_{++} = \rho_{--} = e^{-\beta\nu}\rho_{11}$, and that (ii) only the state $|+\rangle$ is accessible to the system on the shorter timescale τ_2 over which thermalization with respect to the larger splitting takes place. Indeed, at intermediate times $\tau_2 \ll t \ll \tau_1$, the populations of $|1\rangle$ and $|+\rangle$ are

$$\rho_{11} \approx \frac{1}{\mathcal{Z}_I(\beta)} \quad \text{and} \quad \rho_{++} \approx \frac{e^{-\beta\nu}}{\mathcal{Z}_I(\beta)},$$

(36)

which is simply the Boltzmann distribution for a two-level system. This suggests that the first stage consists of the system thermalizing as if it were a two-level system, with the system later proceeding towards its "correct" equilibrium state, once sufficient time has passed for the Rabi oscillations to have an effect on the density operator.
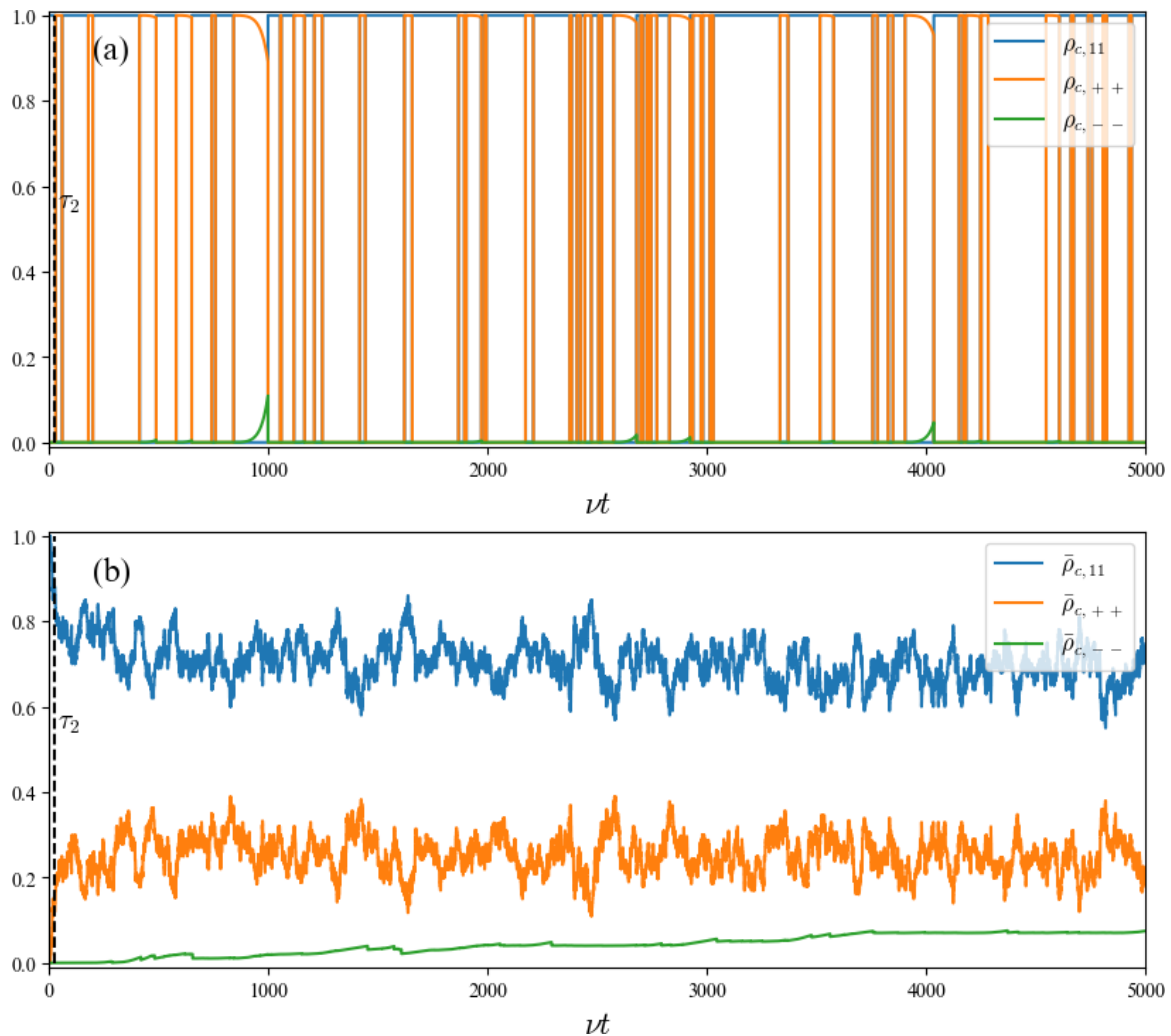
FIG. 9. (a) An example trajectory for the V model in the $\{|1\rangle, |+\rangle, |-\rangle\}$ basis, showing early stages of the dynamics only. A bath-induced jump instantaneously sends the population of $|+\rangle$ (orange) to 1 as the population of $|1\rangle$ (blue) goes to 0, or vice versa. Only once the system has jumped to state $|+\rangle$ can any population reach $|-\rangle$ through Rabi oscillations. Typically, since $\Delta \ll \nu$, this process is interrupted by a jump back down to $|1\rangle$ well before a single period of the Rabi oscillations is completed. (b) One hundred such trajectories, averaged. This averaging recovers the density operator given by quantum master equations, with noise due to the limited size of the sample. Parameter values are the same as in Fig. 7.

IV. DISCUSSION

We have investigated two situations in which open quantum systems with nearly degenerate eigenstates exhibit a dramatic separation of timescales, and associated long-lived coherences, in the process of relaxation towards equilibrium. These effects are captured when dynamics are modelled using the unified quantum master equation, which is better suited to such systems than the fully secular master equation. In examples, we have considered quantum systems interacting with bosonic baths with Ohmic spectral density. However, these choices were made only for the purposes of calculating transition rates, and are not essential to the observation or explanation of the phenomena under investigation. Our approach towards gaining insight as to the physics underlying these timescale effects has been twofold.

Firstly, we have considered how transforming to different bases can reveal different characteristics of the time evolution.

In particular, when the system part of the system-bath interaction Hamiltonian takes on a nontrivial, nondiagonal form, the energy eigenbasis may not be the only natural basis in which to study the dynamics. Transforming to a basis that simplifies the interaction Hamiltonian and/or Lindblad operators can lead to simplified expressions for the state as a function of time and aid in the analysis.

Secondly, using a QME that is of Lindblad form has allowed us to straightforwardly simulate quantum trajectories consistent with these dynamics. While the reduced density operator takes into account the presence or absence of phase coherence between separate instantiations of a quantum system interacting with a bath, individual trajectories, in a sense, provide a more insightful visualization of the underlying dynamics, with randomly timed jumps punctuating periods of coherent evolution.

The presence of nearly degenerate levels in an open quantum system means that, up to leading order in the small

splitting between them, which we have denoted Δ, the reduced density operator at equilibrium is maximally mixed with respect to the nearly degenerate subspace. As such, it will be invariant under any basis transformation that only affects states within this subspace, mimicking the "basis freedom" that occurs for systems with strict degeneracies. For this reason, while the system Hamiltonian technically does specify a unique energy eigenbasis, using a basis chosen by considering the system-bath interaction leads to a clearer understanding of the distinct timescales that arise in the evolution. This was seen very directly in Sec. II, where it turned out that the interaction between our two-level system and its bath could be interpreted as simple decoherence, but into a basis other than the energy eigenbasis. The long-lived coherence, therefore, is highly analogous to spurious coherences that might arise when investigating quantum systems with strict degeneracies, but which are uncontroversially explained away in these scenarios with an appeal to the well-understood basis freedom.

In Sec. III, we considered the case where dissipative dynamics excite jumps over finite-energy splittings between distinct nearly degenerate subspaces, giving rise to a set of nonsimultaneously diagonalizable Lindblad operators. The system-bath interaction could not, therefore, be interpreted as pure decoherence in any basis. However, the same type of basis freedom was employed to identify a basis more natural for describing the dynamics, without having any effect on the reduced density operator at equilibrium. This amounted to identifying, within the nearly degenerate subspace, a pair of orthogonal states, of which one is directly involved in the dissipative dynamics and one is not. Once again, this led to some clarity surrounding the existence of distinct timescales in the dynamics, as it elucidated the fact that the shorter timescale is associated more closely with the dissipative part of the dynamics only, while the longer timescale characterizes effects that involve an interplay between the coherent dynamics (Rabi oscillations) and the dissipative dynamics.

For both cases considered, changes of basis lent themselves well to the inspection of quantum trajectories, as differences between how different matrix elements evolve at the trajectory level, both qualitatively and quantitatively, reflect the different timescales that show up in the expressions for the nonconditional reduced density matrix elements. Certain open questions do, however, remain. For instance, while it is immediately evident by inspecting the trajectories for the two-level system in Fig. 4 how an average of many statistically similar trajectories would recover the curves in Fig. 3, the same cannot quite be said of those for the V model in Fig. 9. Looking at a single trajectory, it appears that the population of $|-\rangle$ only very rarely has a chance to increase beyond about 0.01 or 0.02 before a jump occurs, resetting it to zero. It therefore seems unintuitive that at steady state, this population gets as high as $e^{-\beta v}/\mathcal{Z}(\beta)$ (about 0.21 for the parameter values plotted). This is not to dispute the results of the calculations, just to emphasize the limitations of building intuition by studying an individual trajectory in a particular basis while the reduced density operator is really an ensemble average of infinitely many.

We wish to distinguish these results from related study investigating the presence of coherence at steady state in nonequilibrium situations for open quantum systems that include near degeneracies [42,59,60]. Employing the framework of quantum trajectories to gain insight into the physical processes underlying these steady-state coherences remains an open direction for future research. Furthermore, it is worth noting that recent studies have worked towards establishing methods of obtaining quantum trajectories even if the dynamics are described by non-GKLS-form master equations [67,68]. Such methods would, in principle, allow analyses like this for systems even when no GKLS-form master equation serves as a valid approximation for the dynamics.

APPENDIX: LAMB SHIFT

In general, the unified quantum master equation includes a contribution associated with the Lamb shift [31]. This contribution appears in the unitary part of the evolution and effectively adds an additional term, H_{LS}, to the system Hamiltonian H_S, taking the UQME to

$$\frac{d\rho}{dt} = \mathcal{L}\rho = -i[H_S + H_{LS}, \rho] + \sum_i \mathcal{D}[L_i]\rho, \qquad \text{(A1)}$$

where the summation runs over each collapse operator L_i. For the models we consider, the Lamb shift Hamiltonian itself is constructed of contributions proportional to products of contributions to the system coupling operator, $S_{\omega'}^\dagger S_\omega$ where $|\omega - \omega'| \lesssim \Delta$, and

$$S_\omega = \sum_{j,j';\epsilon_j - \epsilon_{j'}=\omega} P_{j'} S P_j, \qquad \text{(A2)}$$

where P_j is a projector onto an energy eigenstate with energy ϵ_j.

We will briefly consider the role of the Lamb shift in each of the cases studied. Note that for a given model, the Lamb shift Hamiltonian differs between the two bases considered by more than just the basis transformation itself. This is because the transformation can be understood to change how the various elements of the total Hamiltonian manifest in the unitary or dissipative part of the dynamics. Furthermore, while energy splittings of order Δ are neglected in constructing the dissipative part, it is often advantageous to retain them in constructing a "refined" Lamb shift [31]. Accordingly, the choice of basis amounts, in part, to a choice of the extent to which small energy splittings are accounted for explicitly.

For the two-level system, in the energy eigenbasis, the Lamb shift contains off-diagonal elements describing coherent tunneling between the two levels. It is possible to show,

however, that this element is given by

$$\langle 1|H_{LS}|0\rangle = \frac{1}{2i}(\gamma(-\Delta, \Delta) - \gamma(0, 0)). \qquad (A3)$$

By inspection, the magnitude of this element is $\mathcal{O}(\Delta)$, and therefore "small" by the standards stipulated in this paper.

The diagonal elements are given by the imaginary parts of half Fourier transforms of the bath autocorrelation function, evaluated at the splitting. We denote these half Fourier transforms using the symbol Γ e.g.,

$$\langle 1|H_{LS}|1\rangle = \text{Im}[\Gamma(\Delta)],$$

$$\Gamma(\omega) \equiv \int_0^\infty ds \, e^{i\omega s} \text{Tr}[e^{-iH_B s} B^\dagger e^{iH_B s} B \rho_B], \qquad (A4)$$

where ρ_B is the density operator of the bath, given by a Gibbs state at temperature T. Evaluating these integrals using a Drude-Lorenz spectral density with a high cutoff frequency to mimic an Ohmic bath, they are found to take on values smaller than $\sim a\Delta$, where $a \ll 1$ is the dimensionless system-bath coupling constant [42,69]. As such, the Lamb shift serves to increase the energy separation between the two levels, but only by an amount on the order of Δ, leaving the splitting small relative to the temperature scale.

Conversely, in the transformed basis for the two-level system, the system coupling operator takes on a form proportional to σ_z, leaving the only contribution to the Lamb shift Hamiltonian proportional to the identity operator, $\sigma_z^2 = I$, giving rise to no physical effect on the dynamics.

Therefore, while considering the Lamb shift leads to a qualitatively different picture of the system's behavior when studied in the energy eigenbasis (coherent oscillations between eigenstates become possible), the quantitative effects are not significant. For example, relaxation timescales may differ as the eigenstate splitting Δ is augmented by the contribution from H_{LS}, but the small relative size of this contribution

means that the general phenomenon of dramatic timescale separation arises nonetheless. Furthermore, since the Lamb shift has no physical impact in the transformed basis, the procedure outlined in the main text of first transforming to a basis that more naturally captures the system-bath interaction, and only then solving for the dynamics, is unaffected.

The effect of Lamb shift for the V model similarly differs between the two bases considered. In the eigenbasis, there are nonzero off-diagonal elements describing tunneling between eigenstates $|2\rangle$ and $|3\rangle$ of H_S. The real part of this coupling is given by the average of imaginary parts of $\Gamma(\nu - \Delta)$ and $\Gamma(\nu)$, once again shown to be small at relatively high temperatures [42]. The imaginary part of the off-diagonal term, in analogy to Eq. (A3), is manifestly of order-Δ. The levels also shift by amounts given by the imaginary parts of these half Fourier transforms.

In the transformed basis, as for the two-level system, there is no tunneling introduced by the Lamb shift (importantly, the state $|-\rangle$ remains "dark" under the dissipative dynamics and not coupled to state $|1\rangle$ via a tunneling element), leading to the conclusion that the approach of changing basis before deriving the UQME remains a valid approach towards characterizing dramatic timescale separation effects. There is, however, a slight increase to the splitting between levels $|1\rangle$ and $|+\rangle$. In particular, the level $|+\rangle$ shifts by $\text{Im}[\Gamma(\Delta/2 - \nu)]$ while the level $|-\rangle$ is unaffected. Therefore, incorporating the Lamb shift leads to the conclusion that the site energies of $|+\rangle$ and $|-\rangle$ are not equal, as they are if the Lamb shift is neglected. Thus, there is a slight change to the qualitative behavior in this basis: namely, the Rabi oscillations that take place between $|+\rangle$ and $|-\rangle$ must leave at least a small amount of the population in state $|+\rangle$ after a jump up, even in the unlikely case that the oscillation is able to proceed through an entire period uninterrupted by a jump down. This difference in behavior does not, however, diminish the dramatic timescale separation effects that are the focus of this paper.

---

[1] M. Merkli, H. Song, and G. P. Berman, Multiscale dynamics of open three-level quantum systems with two quasi-degenerate levels, J. Phys. A: Math. Theor. **48**, 275304 (2015).

[2] F. Ivander, N. Anto-Sztrikacs, and D. Segal, Hyperacceleration of quantum thermalization dynamics by bypassing long-lived coherences: An analytical treatment, Phys. Rev. E **108**, 014130 (2023).

[3] I. Klich, O. Raz, O. Hirschberg, and M. Vucelja, Mpemba index and anomalous relaxation, Phys. Rev. X **9**, 021060 (2019).

[4] F. Carollo, A. Lasanta, and I. Lesanovsky, Exponentially accelerated approach to stationarity in Markovian open quantum systems through the Mpemba effect, Phys. Rev. Lett. **127**, 060401 (2021).

[5] S. K. Manikandan, Equidistant quenches in few-level quantum systems, Phys. Rev. Res. **3**, 043108 (2021).

[6] S. Kochsiek, F. Carollo, and I. Lesanovsky, Accelerating the approach of dissipative quantum spin systems towards stationarity through global spin rotations, Phys. Rev. A **106**, 012207 (2022).

[7] N. Anto-Sztrikacs, H. J. D. Miller, A. Nazir, and D. Segal, Bypassing thermalization timescales in temperature estimation using prethermal probes, arXiv:2311.05496.

[8] T. V. Tscherbul and P. Brumer, Long-lived quasistationary coherences in a V-type system driven by incoherent light, Phys. Rev. Lett. **113**, 113601 (2014).

[9] T. V. Tscherbul and P. Brumer, Partial secular Bloch-Redfield master equation for incoherent excitation of multilevel quantum systems, J. Chem. Phys. **142**, 104107 (2015).

[10] A. Dodin, T. Tscherbul, R. Alicki, A. Vutha, and P. Brumer, Secular versus nonsecular Redfield dynamics and Fano coherences in incoherent excitation: An experimental proposal, Phys. Rev. A **97**, 013421 (2018).

[11] M. A. Nielsen and I. L. Chuang, *Quantum Computation and Quantum Information: 10th Anniversary Edition* (Cambridge University Press, Cambridge, 2010).

[12] M. O. Scully, K. R. Chapin, K. E. Dorfman, and A. Svidinsky, Quantum heat engine power can be increased by noise-induced coherence, Proc. Natl. Acad. Sci. USA **108**, 15097 (2011).

[13] M. Kilgour and D. Segal, Coherence and decoherence in quantum absorption refrigerators, Phys. Rev. E **98**, 012117 (2018).

[14] K. Hammam, Y. Hassouni, R. Fazio, and G. Manzano, Optimizing autonomous thermal machines powered by energetic coherence, New J. Phys. **23**, 043024 (2021).

[15] J. Um, K. E. Dorfman, and H. Park, Coherence-enhanced quantum-dot heat engine, Phys. Rev. Res. **4**, L032034 (2022).

[16] B. K. Agarwalla and D. Segal, Assessing the validity of the thermodynamic uncertainty relation in quantum systems, Phys. Rev. B **98**, 155438 (2018).

[17] J. Liu and D. Segal, Coherences and the thermodynamic uncertainty relation: Insights from quantum absorption refrigerators, Phys. Rev. E **103**, 032138 (2021).

[18] M. Gerry and D. Segal, Absence and recovery of cost-precision tradeoff relations in quantum transport, Phys. Rev. B **105**, 155401 (2022).

[19] G. S. Engel, T. R. Calhoun, E. L. Read, T.-K. Ahn, T. Mančal, Y.-C. Cheng, R. E. Blankenship, and G. R. Fleming, Evidence for wavelike energy transfer through quantum coherence in photosynthetic systems, Nature (London) **446**, 782 (2007).

[20] I. Kassal, J. Yuen-Zhou, and S. Rahimi-Keshari, Does coherence enhance transport in photosynthesis? J. Phys. Chem. Lett. **4**, 362 (2013).

[21] V. I. Prokhorenko, A. M. Nagy, S. A. Waschuk, L. S. Brown, R. R. Birge, and R. J. D. Miller, Coherent control of retinal isomerization in bacteriorhodopsin, Science **313**, 1257 (2006).

[22] T. V. Tscherbul and P. Brumer, Quantum coherence effects in natural light-induced processes: *cis-trans* photoisomerization of model retinal under incoherent excitation, Phys. Chem. Chem. Phys. **17**, 30904 (2015).

[23] D. Kohen, C. C. Marston, and D. J. Tannor, Phase space approach to theories of quantum dissipation, J. Chem. Phys. **107**, 5236 (1997).

[24] R. Hartmann and W. T. Strunz, Accuracy assessment of perturbative master equations: Embracing nonpositivity, Phys. Rev. A **101**, 012103 (2020).

[25] G. Argentieri, F. Benatti, R. Floreanini, and M. Pezzutto, Violations of the second law of thermodynamics by a non-completely positive dynamics, Europhys. Lett. **107**, 50007 (2014).

[26] M. Gerry and D. Segal, Full counting statistics and coherences: Fluctuation symmetry in heat transport with the unified quantum master equation, Phys. Rev. E **107**, 054115 (2023).

[27] V. Gorini, A. Kossakowski, and E. C. G. Sudarshan, Completely positive dynamical semigroups of *N*-level systems, J. Math. Phys. **17**, 821 (1976).

[28] G. Lindblad, On the generators of quantum dynamical semigroups, Commun. Math. Phys. **48**, 119 (1976).

[29] H.-P. Breuer and F. Petruccione, *The Theory of Open Quantum Systems* (Oxford University Press, Oxford, 2002).

[30] E. B. Davies, Markovian master equations, Commun. Math. Phys., **39** 91 (1974).

[31] A. Trushechkin, Unified Gorini-Kossakowski-Lindblad-Sudarshan quantum master equation beyond the secular approximation, Phys. Rev. A **103**, 062226 (2021).

[32] G. McCauley, B. Cruikshank, D. I. Bondar, and K. Jacobs, Accurate Lindblad-form master equation for weakly damped quantum systems across all regimes, npj Quantum Inf. **6**, 74 (2020).

[33] P. P. Potts, A. A. S. Kalaee, and A. Wacker, A thermodynamically consistent Markovian master equation beyond the secular approximation, New J. Phys. **23**, 123013 (2021).

[34] D. Farina and V. Giovannetti, Open-quantum-system dynamics: Recovering positivity of the Redfield equation via the partial secular approximation, Phys. Rev. A **100**, 012107 (2019).

[35] J. Jeske, D. J. Ing, M. B. Plenio, S. F. Huelga, and J. H. Cole, Bloch-Redfield equations for modeling light-harvesting complexes, J. Chem. Phys. **142**, 064104 (2015).

[36] A. Soret, V. Cavina, and M. Esposito, Thermodynamic consistency of quantum master equations, Phys. Rev. A **106**, 062209 (2022).

[37] G. C. Hegerfeldt and M. B. Plenio, Macroscopic dark periods without a metastable state, Phys. Rev. A **46**, 373 (1992).

[38] G. C. Hegerfeldt and M. B. Plenio, Coherence with incoherent light: A new type of quantum beat for a single atom, Phys. Rev. A **47**, 2186 (1993).

[39] S. Hernández-Gómez, S. Gherardini, N. Staudenmaier, F. Poggiali, M. Campisi, A. Trombettoni, F. S. Cataliotti, P. Cappellaro, and N. Fabbri, Autonomous dissipative Maxwell's demon in a diamond spin qutrit, PRX Quantum **3**, 020329 (2022).

[40] A. Dodin, T. V. Tscherbul, and P. Brumer, Quantum dynamics of incoherently driven *V*-type systems: Analytic solutions beyond the secular approximation, J. Chem. Phys. **144**, 244108 (2016).

[41] S.-W. Li, C. Y. Cai, and C. P. Sun, Steady quantum coherence in non-equilibrium environment, Ann. Phys. (NY) **360**, 19 (2015).

[42] F. Ivander, N. Anto-Sztrikacs, and D. Segal, Quantum coherence-control of thermal energy transport: The V model as a case study, New J. Phys. **24**, 103010 (2022).

[43] F. Minganti, A. Miranowicz, R. W. Chhajlany, and F. Nori, Quantum exceptional points of non-Hermitian Hamiltonians and Liouvillians: The effects of quantum jumps, Phys. Rev. A **100**, 062131 (2019).

[44] S. Khandelwal, N. Brunner, and G. Haack, Signatures of Liouvillian exceptional points in a quantum thermal machine, PRX Quantum **2**, 040346 (2021).

[45] A. Dodin and P. Brumer, Noise-induced coherence in molecular processes, J. Phys. B **54**, 223001 (2021).

[46] S. Koyu and T. V. Tscherbul, Long-lived quantum coherences in a *V*-type system strongly driven by a thermal environment, Phys. Rev. A **98**, 023811 (2018).

[47] S. Koyu and T. V. Tscherbul, Long-lived quantum coherent dynamics of a Λ-system driven by a thermal environment, J. Chem. Phys. **157**, 124302 (2022).

[48] C. W. Gardiner, A. S. Parkins, and P. Zoller, Wave-function quantum stochastic differential equations and quantum-jump simulation methods, Phys. Rev. A **46**, 4363 (1992).

[49] H. Wiseman and G. J. Milburn, *Quantum Measurement and Control* (Cambridge University Press, Cambridge, 2009).

[50] K. Jacobs, *Quantum Measurement Theory and its Applications* (Cambridge University Press, Cambridge, 2014).

[51] G. T. Landi, M. J. Kewming, M. T. Mitchison, and P. P. Potts, Current fluctuations in open quantum systems: Bridging the gap between quantum continuous measurements and full counting statistics, PRX Quantum **5**, 020201 (2024).

[52] M. Rigo, F. Mota-Furtado, and P. O'Mahony, Continuous stochastic Schrödinger equations and localization, J. Phys. A: Math. Gen. **30**, 7557 (1997).

[53] M. Hofmann and B. Drossel, Dephasing versus collapse: Lessons from the tight-binding model with noise, New J. Phys. **23**, 103025 (2021).

[54] K. Maciesczzak, M. Guţă, I. Lesanovsky, and J. P. Garrahan, Towards a theory of metastability in open quantum dynamics, Phys. Rev. Lett. **116**, 240404 (2016).

[55] K. Maciesczzak, D. C. Rose, I. Lesanovsky, and J. P. Garrahan, Theory of classical metastability in open quantum systems, Phys. Rev. Res. **3**, 033047 (2021).

[56] S. Matern, K. Maciesczzak, S. Wozny, and M. Leijnse, Metastability and quantum coherence assisted sensing in interacting parallel quantum dots, Phys. Rev. B **107**, 125424 (2023).

[57] C. A. Brown, K. Maciesczzak, and R. L. Jack, Unraveling metastable Markovian open quantum systems, Phys. Rev. A **109**, 022244 (2024).

[58] D. C. Rose, H. Touchette, I. Lesanovsky, and J. P. Garrahan, Spectral properties of simple classical and quantum reset processes, Phys. Rev. E **98**, 022129 (2018).

[59] G. Guarnieri, M. Kolář, and R. Filip, Steady-state coherences by composite system-bath interactions, Phys. Rev. Lett. **121**, 070401 (2018).

[60] A. Purkayastha, G. Guarnieri, M. T. Mitchison, R. Filip, and J. Goold, Tunable phonon-induced steady-state coherence in a double-quantum-dot charge qubit, npj Quantum Inf **6**, 27 (2020).

[61] N. Anto-Sztrikacs, F. Ivander, and D. Segal, Quantum thermal transport beyond second order with the reaction coordinate mapping, J. Chem. Phys. **156**, 214107 (2022).

[62] D. Segal, Single mode heat rectifier: Controlling energy flow between electronic conductors, Phys. Rev. Lett. **100**, 105901 (2008).

[63] J. R. Johansson, P. D. Nation, and F. Nori, QuTiP: An open-source Python framework for the dynamics of open quantum systems, Comput. Phys. Commun. **183**, 1760 (2012).

[64] J. R. Johansson, P. D. Nation, and F. Nori, QuTiP 2: A Python framework for the dynamics of open quantum systems, Comput. Phys. Commun. **184**, 1234 (2013).

[65] A. De Gregorio and F. Iafrate, Telegraph random evolutions on a circle, Stochastic Process. Appl. **141**, 79 (2021).

[66] C. Gardiner and P. Zoller, *Quantum Noise* (Springer, New York, 2004).

[67] B. Donvil and P. Muratore-Ginanneschi, Quantum trajectory framework for general time-local master equations, Nat. Commun. **13**, 4140 (2022).

[68] T. Becker, C. Netzer, and A. Eckardt, Quantum trajectories for time-local non-Lindblad master equations, Phys. Rev. Lett. **131**, 160401 (2023).

[69] J. Thingna, J. L. García-Palacios, and J.-S. Wang, Steady-state thermal transport in anharmonic systems: Application to molecular junctions, Phys. Rev. B **85**, 195452 (2012).